Supporting Information

for

Textured nanoporous Mo:$BiVO_4$ photoanodes with high charge transport and charge transfer quantum efficiencies for oxygen evolution

*Vineet Nair,[1] Craig L. Perkins,[2] Qiyin Lin,[3] Matt Law[1,3,4,]**
[1] Department of Chemical Engineering and Materials Science, University of California, Irvine, Irvine, CA 92697
[2] National Renewable Energy Laboratory, Golden, CO 80401
[3] Laboratory for Electron and X-ray Instrumentation, University of California, Irvine, Irvine, CA 92697
[4] Department of Chemistry, University of California, Irvine, Irvine, CA 92697

*corresponding author: Matt Law; email: matt.law@uci.edu

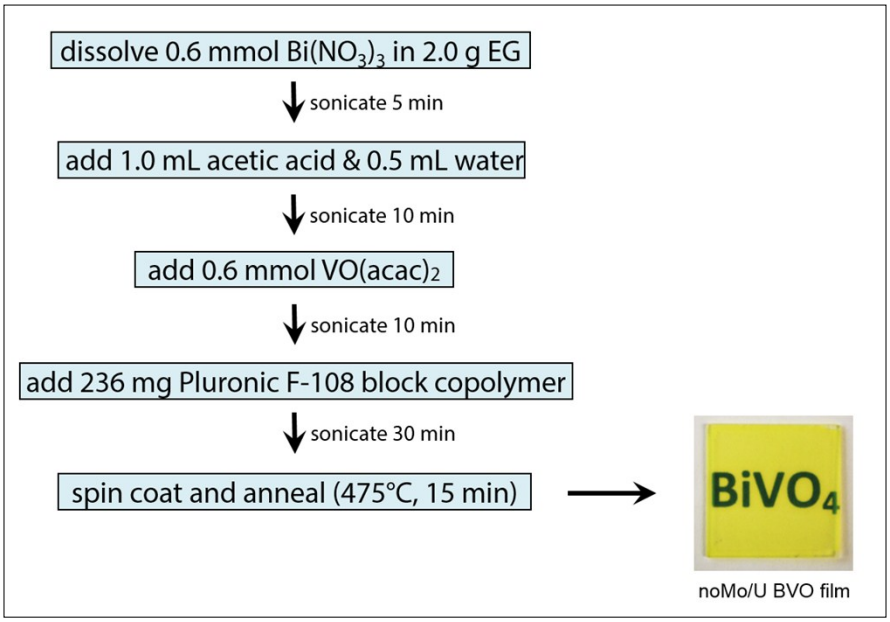

Scheme 1. Fabrication flow diagram for "noMo/U" BVO films.

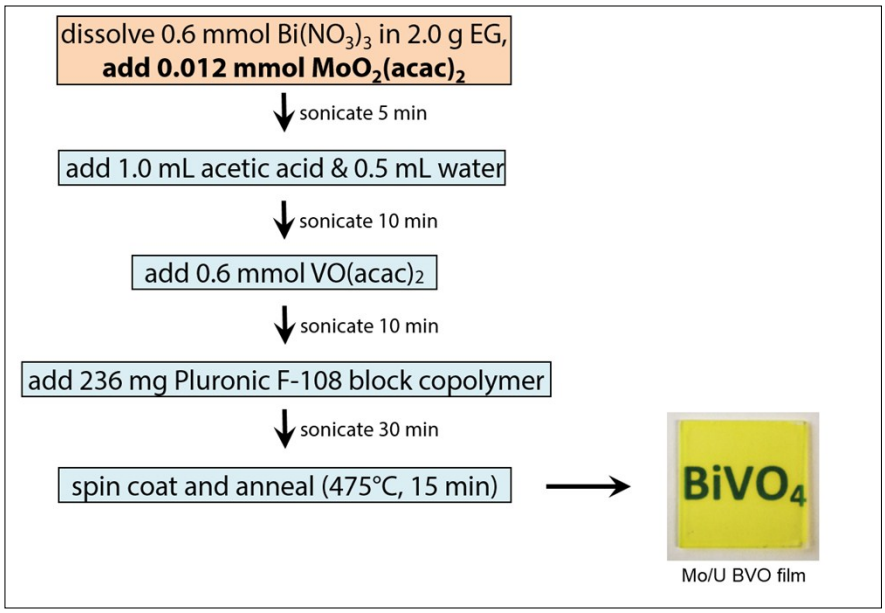

Scheme 2. Fabrication flow diagram for "Mo/U" BVO films.

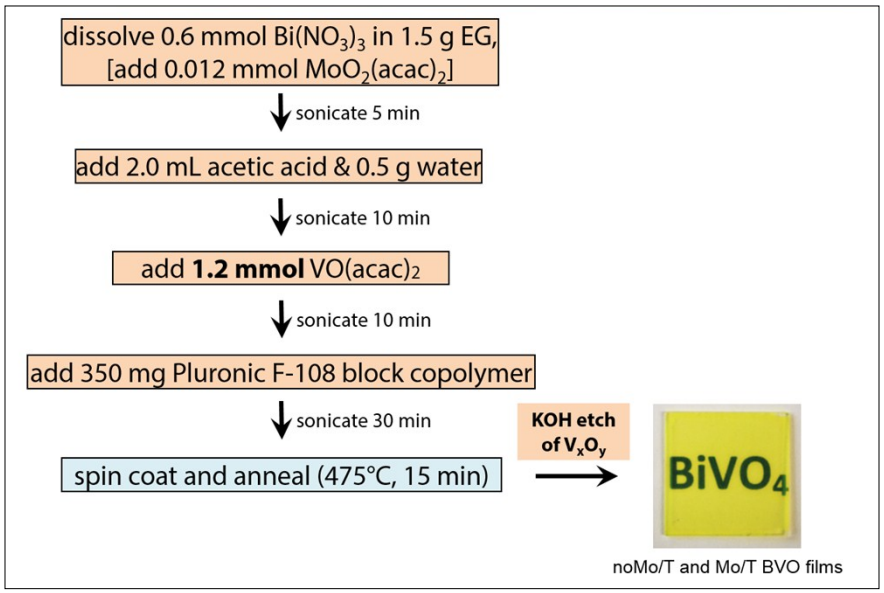

Scheme 3. Fabrication flow diagram for "noMo/T" and "Mo/T" BVO films.

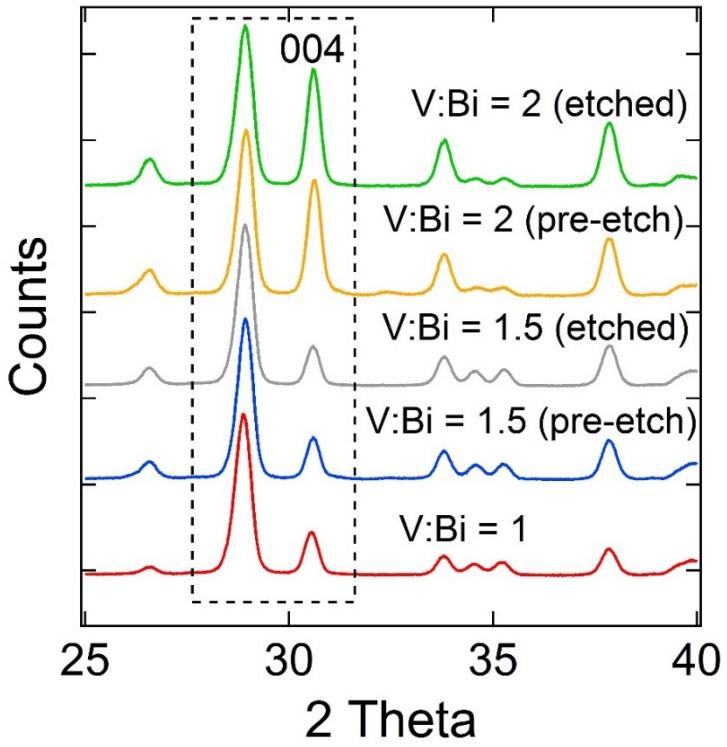

Figure S1. GIXRD patterns of BVO films made on FTO-coated glass substrates from inks with different [V]/[Bi] ratios. To remove V_xO_y impurities, some of the films were etched in 0.5 *M* aqueous KOH for 10 seconds, then rinsed with deionized water and dried under a stream of nitrogen. Hashed box shows appearance of 004 texture at [V]/[Bi] = 2.

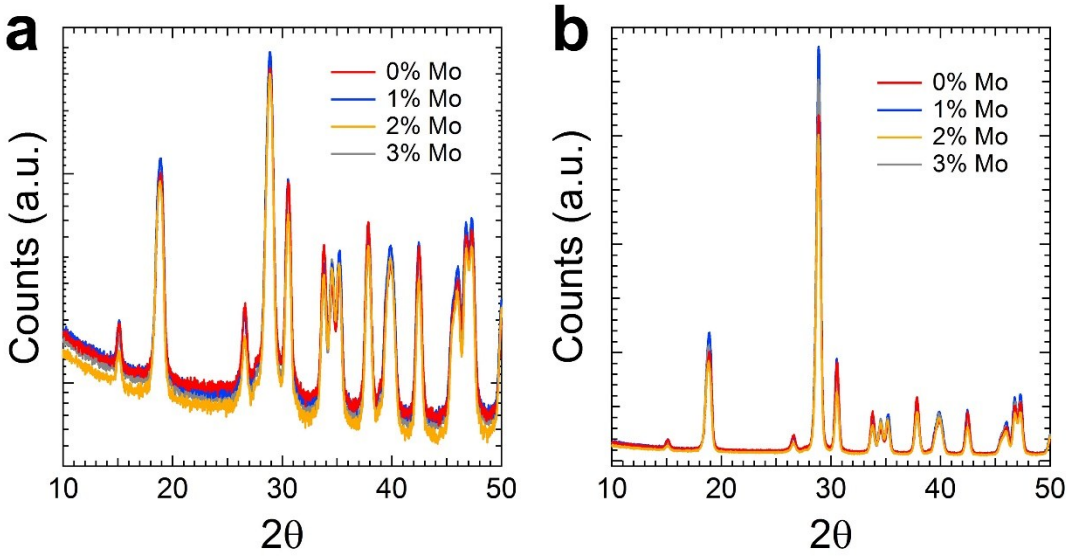

Figure S2. GIXRD patterns of BVO films made on FTO-coated glass substrates from inks containing different concentrations of $MoO_2(acac)_2$. (a) The data on a log scale. (b) The data on a linear scale.

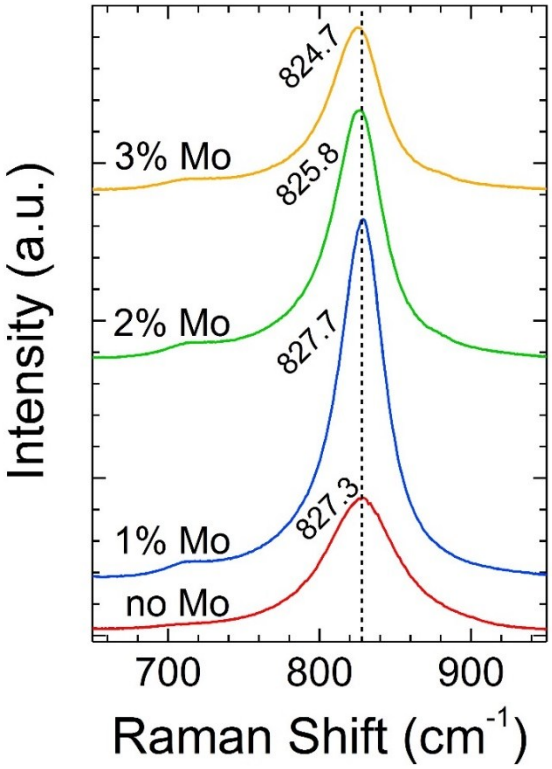

Figure S3. Raman spectra of textured BVO films as a function of the Mo content of the ink.

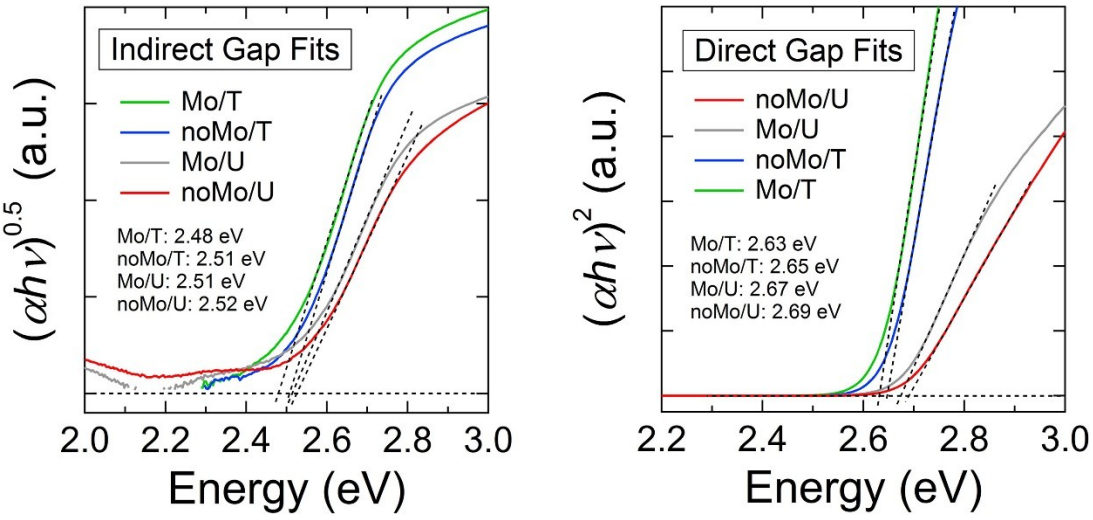

Figure S4. Tauc plots of the four types of BVO films on FTO-coated glass substrates assuming an indirect band gap (*left*) and direct band gap (*right*).

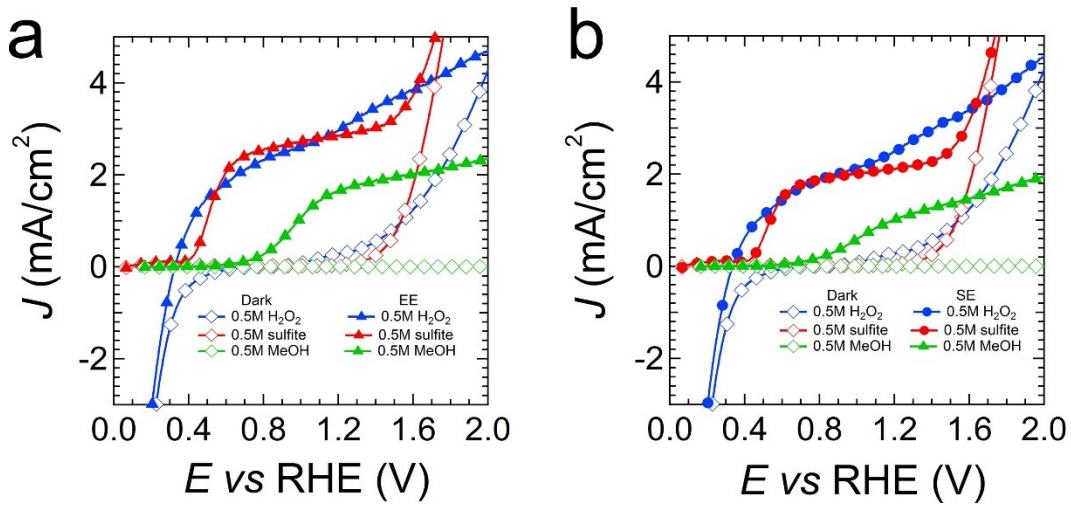

Figure S5. *J-V* curves for Mo/T films in 0.5 *M* K_2SO_4 electrolyte containing 0.5 *M* H_2O_2 (blue), Na_2SO_3 (red), or CH_3OH (green). (a) Data for EE illumination. (b) Data for SE illumination.

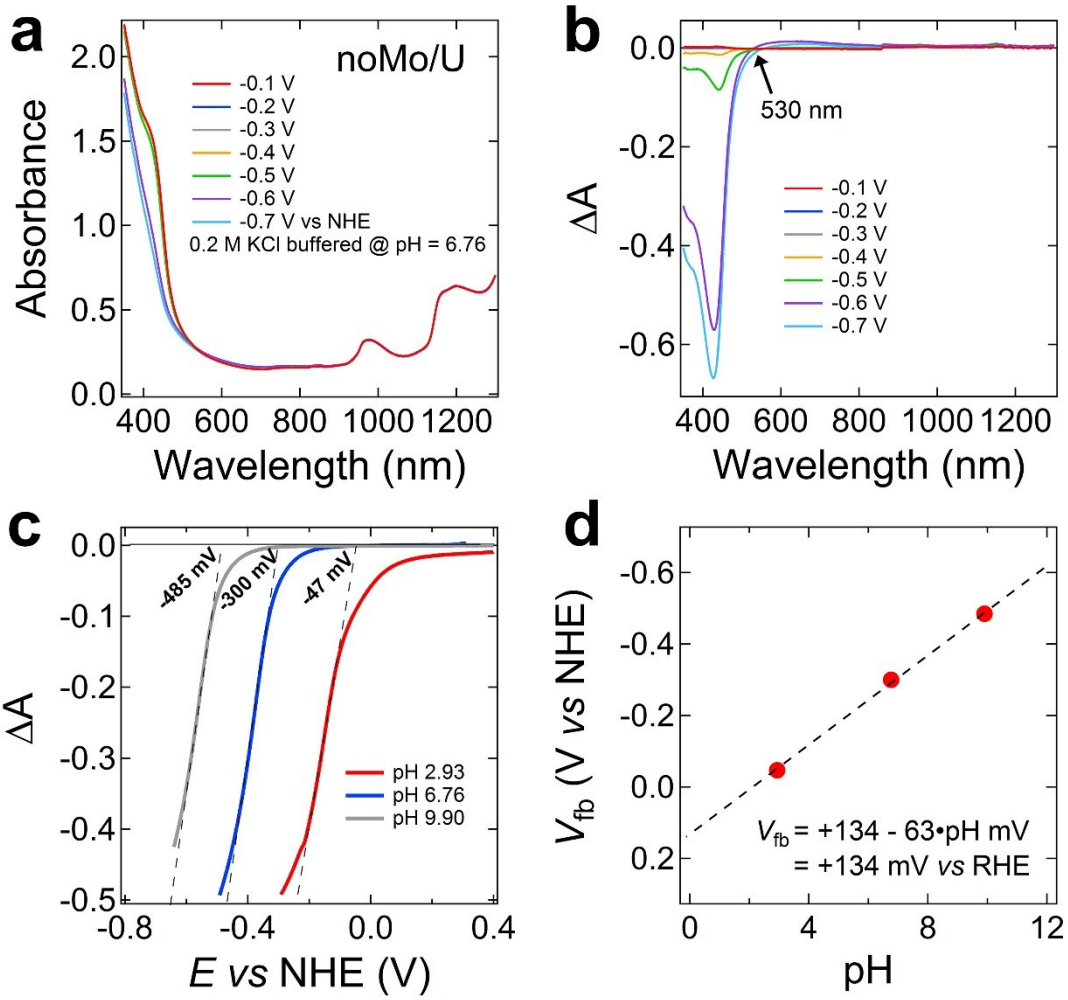

Figure S6. Determination of the flat band potential (V_{fb}) of noMo/U BVO films by room-temperature spectroelectrochemistry. (a) Absorbance spectra of a typical film on an FTO-coated glass substrate as a function of applied bias vs NHE. The film is 450 nm thick and the electrolyte is 0.2 *M* KCl buffered with phosphate to pH 6.76. (b) Difference spectra obtained by subtracting the 0 V spectrum from each of the spectra in (a). There is a spectral bleach above the band gap (Burstein-Moss shift) and a small induced absorption below the band gap (assigned to free carrier absorption). (c) Plots of the absorbance change at 440 nm versus applied bias for films at three different pH values. Linear extrapolation of the data to zero are interpreted as V_{fb} at each pH (e.g., V_{fb} = -485 mV vs NHE at pH 2.93). (d) Plot of V_{fb} versus pH, showing that the flat band potential is Nernstian with a slope of -63 mV/pH. V_{fb} = +134 mV vs RHE.

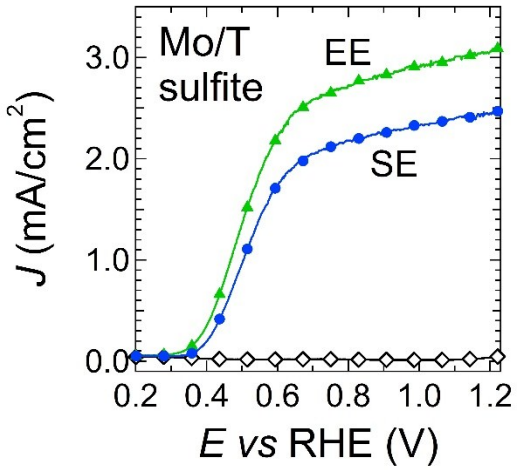

Figure S7. *J-V* curves of a champion (top 10%) Mo/T electrode for sulfite oxidation. The device shows $J = 3.1$ mA cm^{-2} at 1.23 V_{RHE} and 2.2 mA cm^{-2} at 0.6 V_{RHE} under EE illumination.

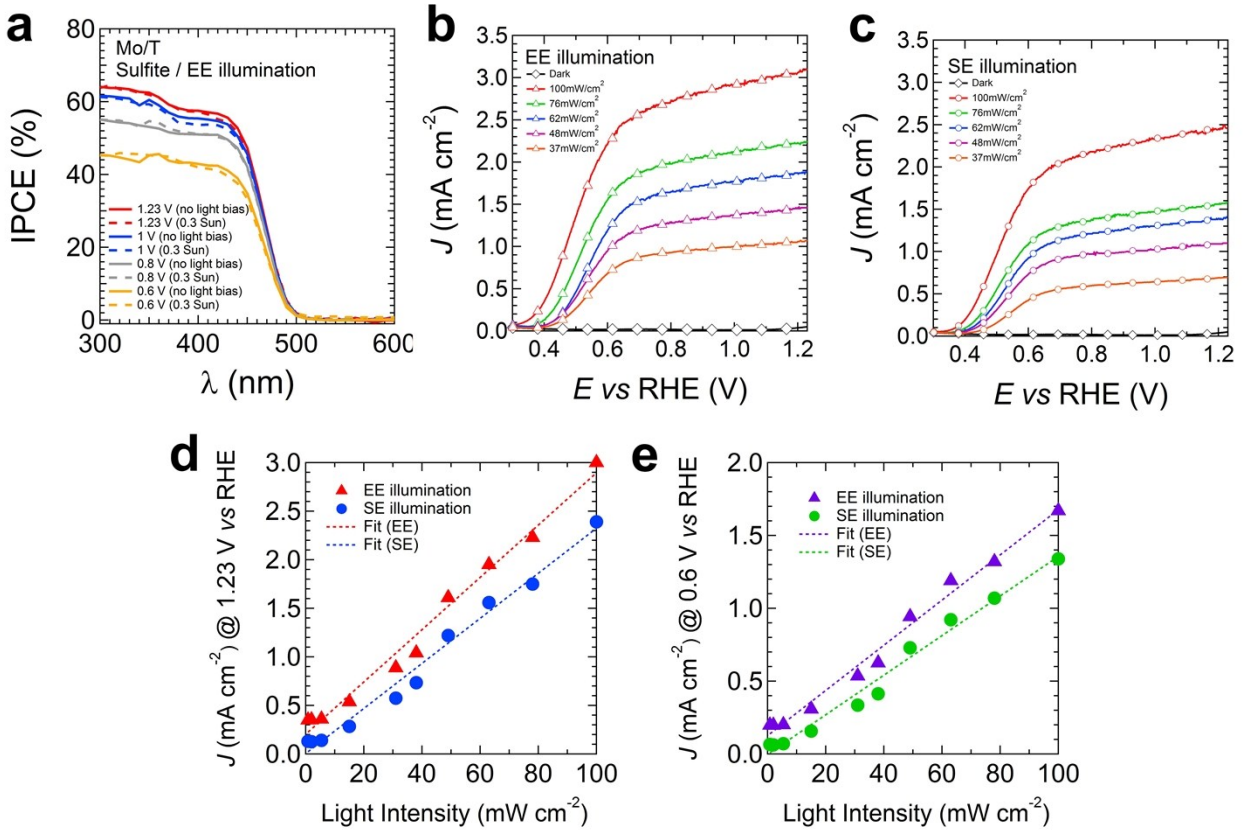

Figure S8. Effect of light intensity on EQE and *J-V* data for Mo/T electrodes in sulfite electrolyte. (a) EQE plots under EE illumination with and without a white light bias of 0.3 sun from the solar simulator. (b-c) *J-V* plots at different light intensities under EE and SE illumination, respectively. (d-e) Corresponding plots of photocurrent vs. light intensity for devices held at a bias of 1.23 V_{RHE} and 0.6 V_{RHE}, respectively.

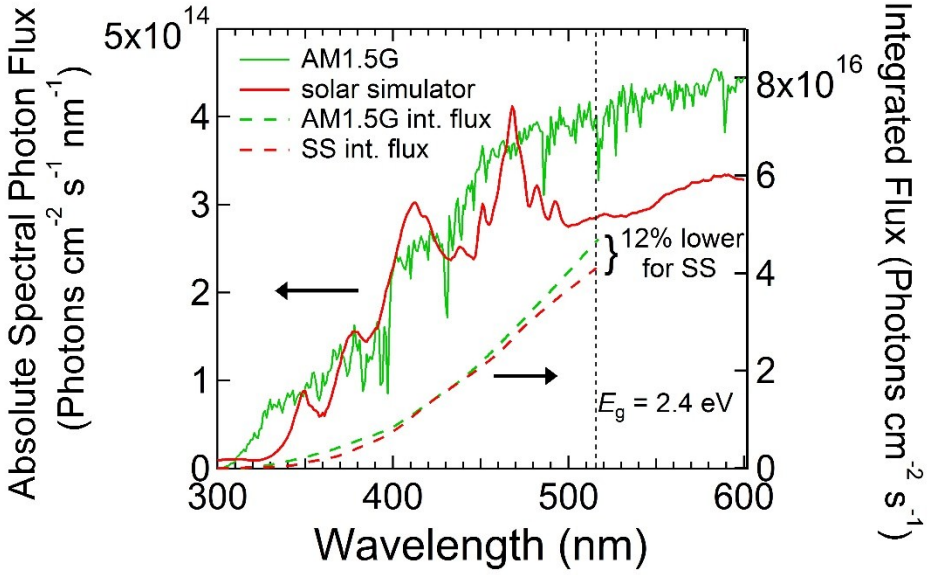

Figure S9. (*left axis*) Absolute spectral photon flux of the standard AM1.5G solar spectrum (green trace) and the solar simulator used to measure *J-V* curves in this work (red trace), measured with a calibrated spectrometer at the sample position. (*right axis*) Integrated photon flux for the AM1.5G spectrum and the solar simulator showing 12% fewer total photons in the solar simulator photon flux over the range of wavelengths relevant to BVO (300-515 nm).

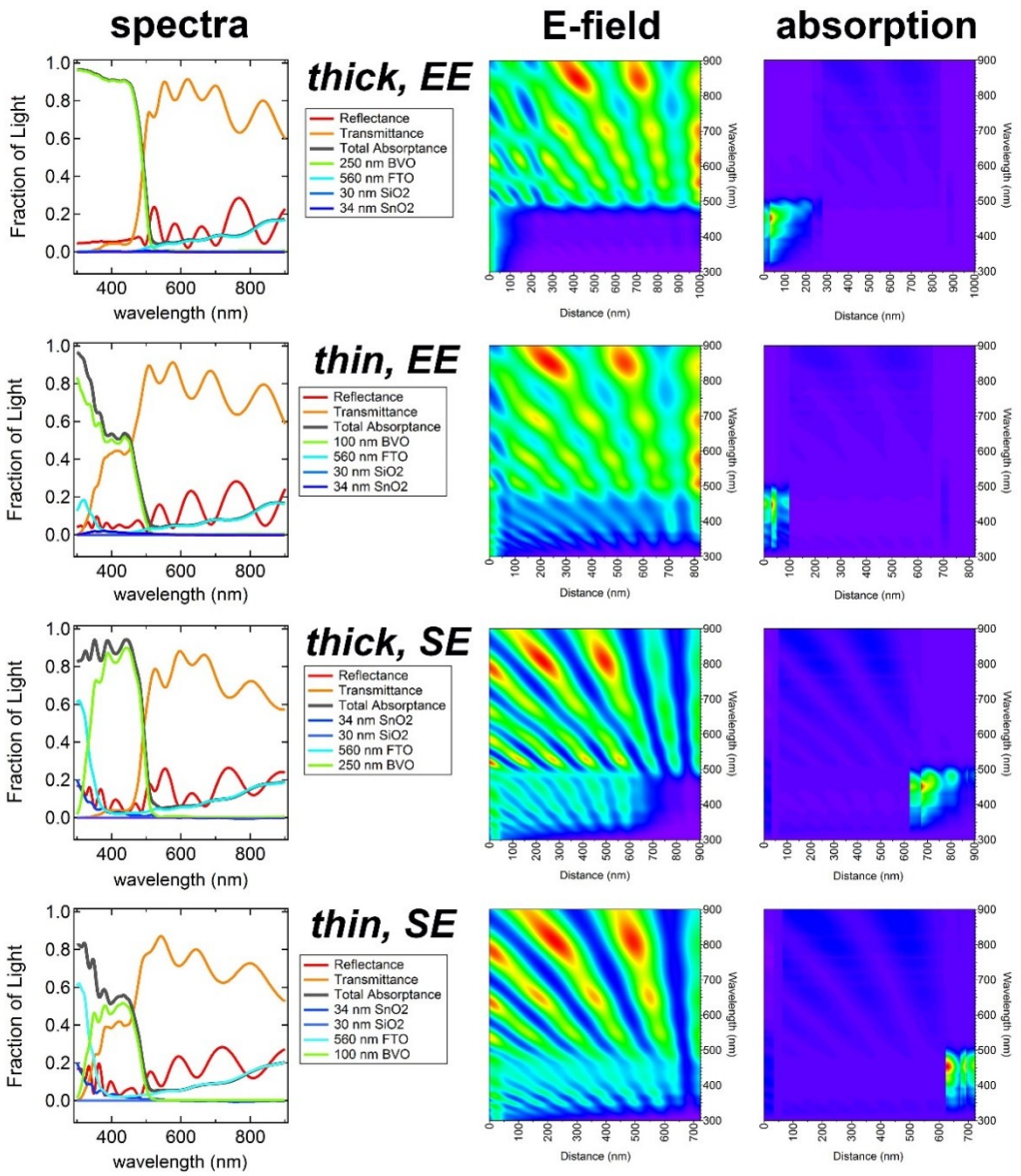

Figure S10. Results of 1D transfer matrix modeling of electrodes with 250 nm ("thick") and 100 nm ("thin") BVO films in both EE and SE illumination. (*left column*) Plots of total reflectance, transmittance, and absorptance, and the absorptance of each layer in the electrode stack for the four situations. The layer sequence for EE illumination is [water]/[30 nm 50:50 BVO:water]/[*x* nm 70:30 BVO:water]/[50 nm 50:50 BVO:FTO]/[560 nm FTO]/[30 nm SiO_2 buffer layer]/[34 nm SnO_2 adhesion layer]/[3 mm glass]/water. The layer sequence for SE illumination is [water]/[3 mm glass]/[34 nm SnO_2 adhesion layer]/[30 nm SiO_2 buffer layer]/[560 nm FTO]/[50 nm 50:50 BVO:FTO]/[*x* nm 70:30 BVO:water]/[30 nm 50:50 BVO:water]/water. x = 170 nm for the thick films and 20 nm for the thin films (giving a total BVO thickness of 250 nm and 100 nm, respectively). (*middle and right columns*) Maps of the absolute square of the electric field and the photon absorption rate for each case. AM1.5G illumination is incident from the left. Optical function of BVO is taken from Ref 1 and TEC 8 glass from Ref 2. Optical functions for the mixed-phase layers were calculated with the Bruggeman effective medium approximation.

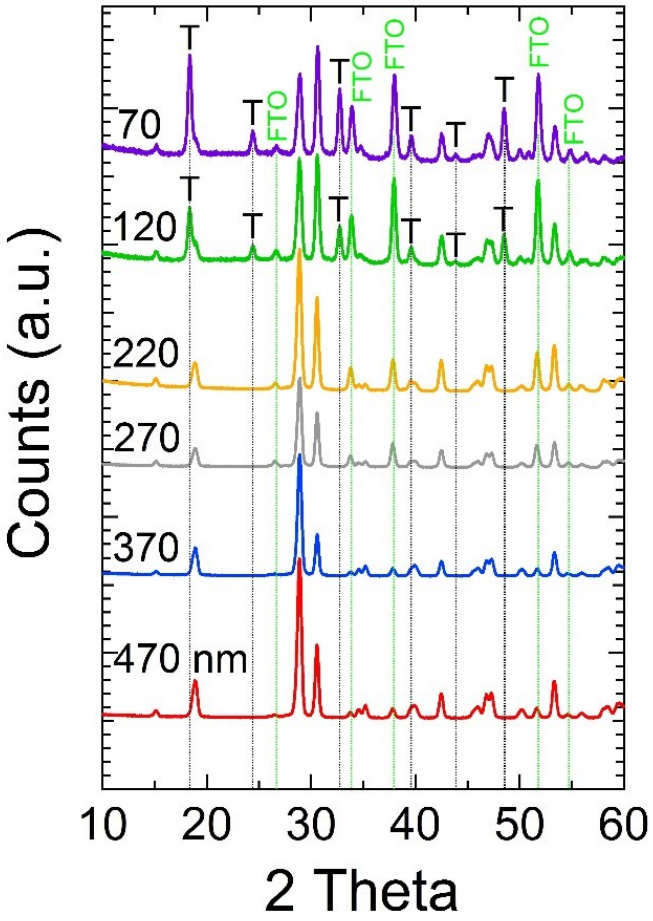

Figure S11. GIXRD patterns of Mo/T films on FTO-coated glass substrates as a function of BVO film thickness. The two thinnest films contain monoclinic and tetragonal (T) $BiVO_4$, while all thicker films show only monoclinic BVO. FTO reflections are also labeled.

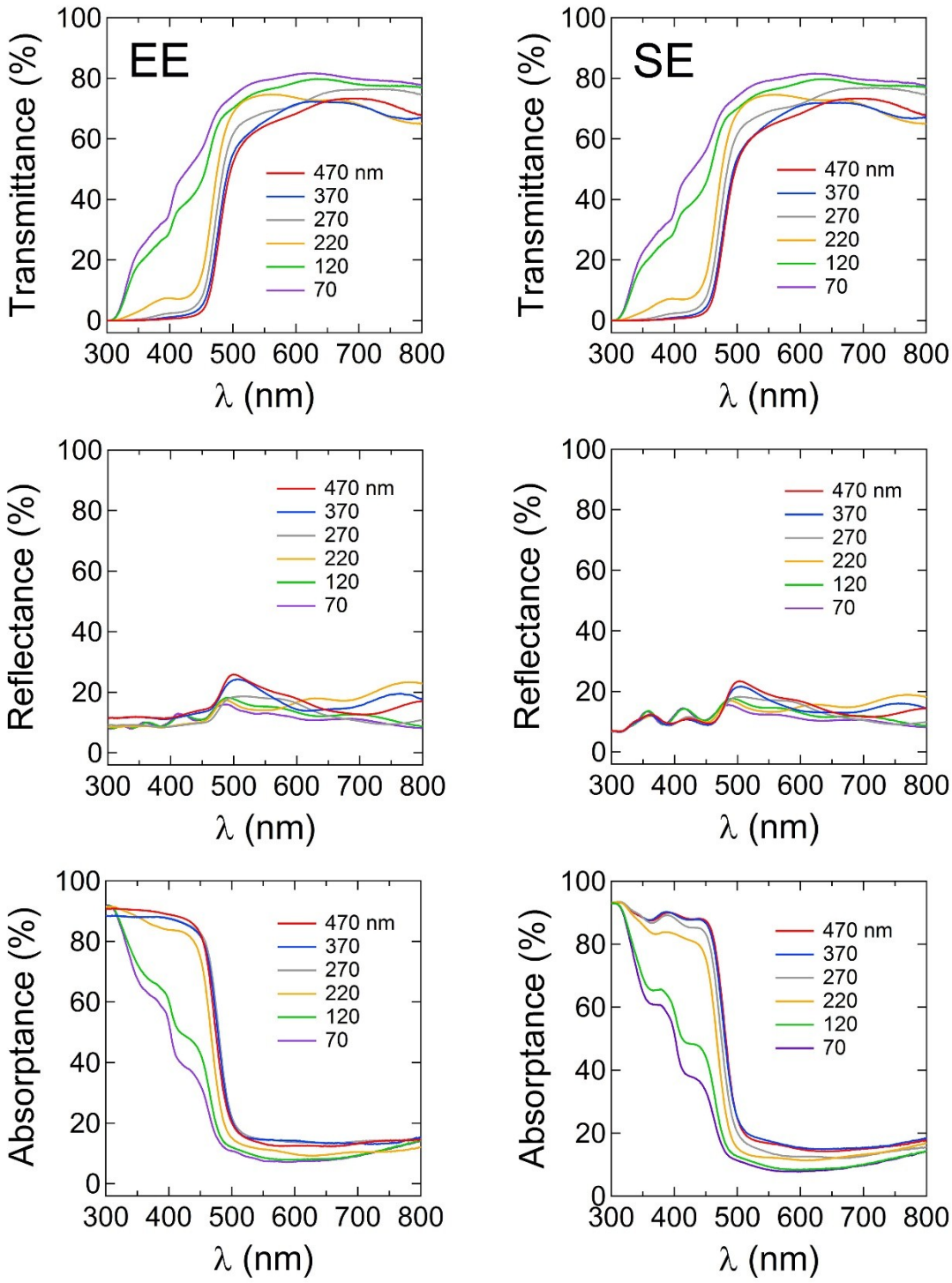

Figure S12. Transmittance, reflectance, and absorptance spectra for Mo/T films on FTO-coated glass substrates as a function of BVO film thickness, as determined using an integrating sphere. (*left column*) EE illumination. (*right column*) SE illumination.

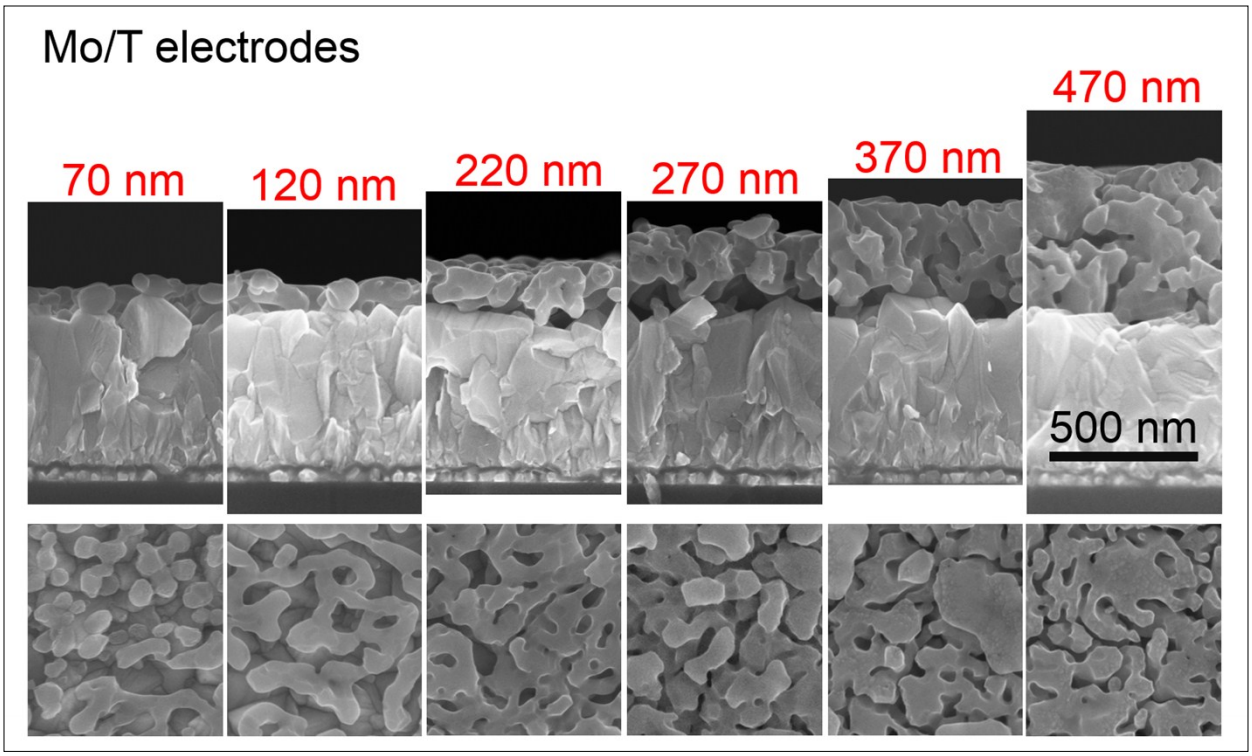

Figure S13. SEM cross sectional and plan view images of Mo/T BVO films on FTO substrates as a function of BVO film thickness. The two thinnest films (120 nm, and especially 70 nm) seem significantly more porous than the thicker films, while the 220-470 nm thick films appear to have about equal porosity. The higher porosity of the two thinnest films may contribute to their worse IQE (e.g., smaller crystallite size resulting in poorer transport), but we believe that the tetragonal BVO phase impurity present in these two films is the more important factor limiting the IQE.

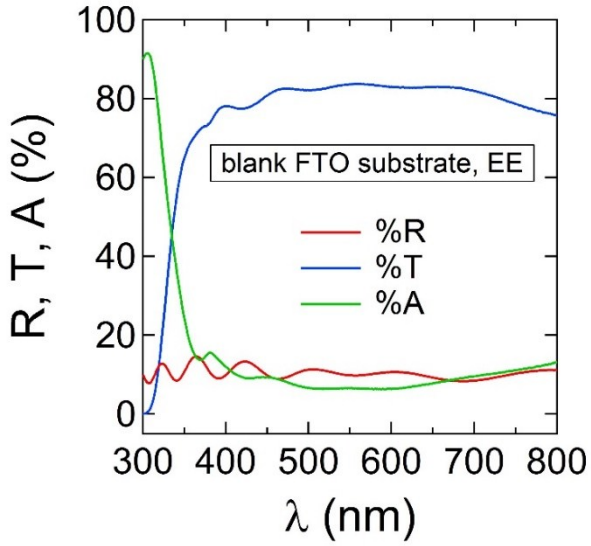

Figure S14. Transmittance, reflectance, and absorptance spectra for a blank FTO-coated glass substrate as determined using an integrating sphere.

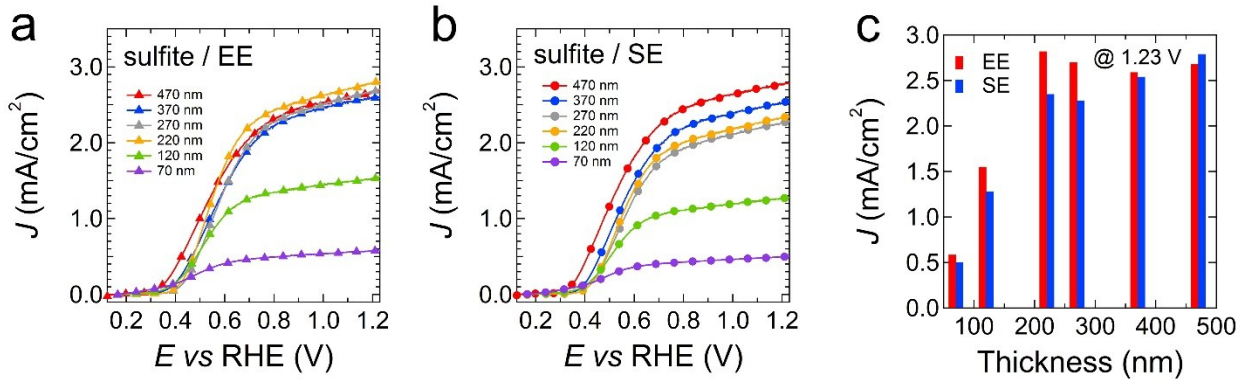

Figure S15. *J-V* plots for sulfite oxidation as a function of BVO film thickness under (a) EE illumination and (b) SE illumination. The onset of photocurrent is ~50 mV more cathodic for the 470 nm thick films. This lower onset is real and reproducible but its cause is unclear. (c) Bar graph of photocurrent at 1.23 V_{RHE} for the Mo/T films in both illumination geometries.

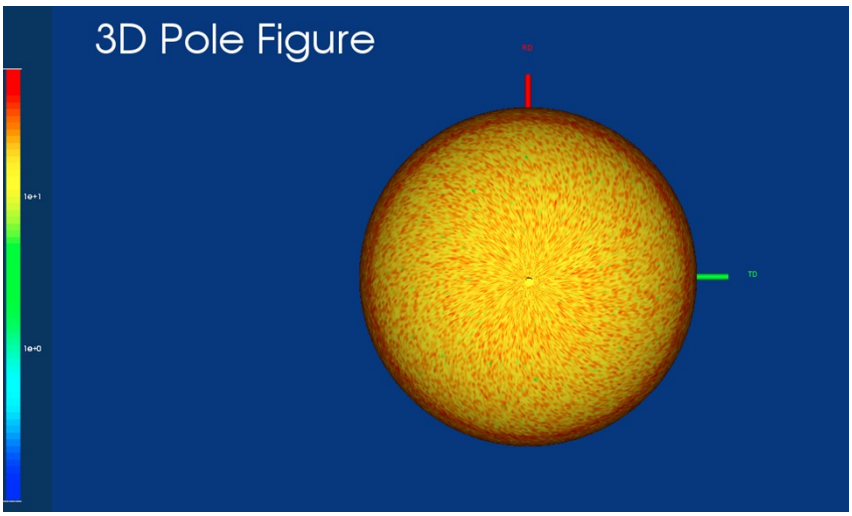

Figure S16. {004} pole figure of a Mo/T film grown on a quartz substrate, showing that the {004} plane normals are distributed preferentially within the plane of the substrate.

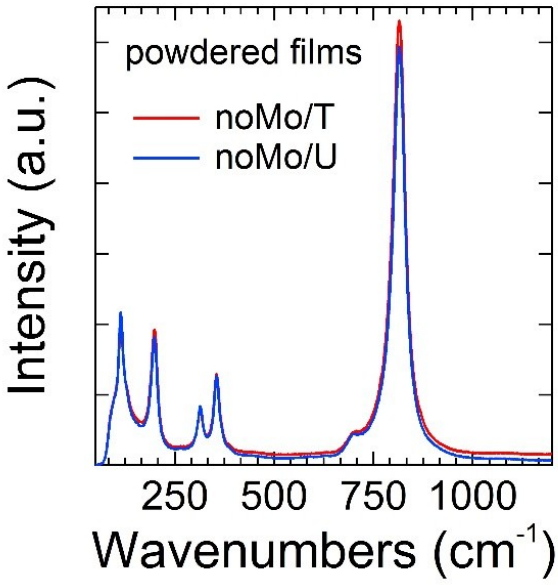

Figure S17. Raman spectra of powdered noMo/T and noMo/U films. The samples were made by scraping a number of films from their substrates and pressing the resulting powders into pellets using a hand press. The spectra are nearly identical, demonstrating that the much larger Raman signal intensity of textured films (Fig. 5) is a result of preferred orientation (texture) rather than more perfect crystallinity or fewer defects.

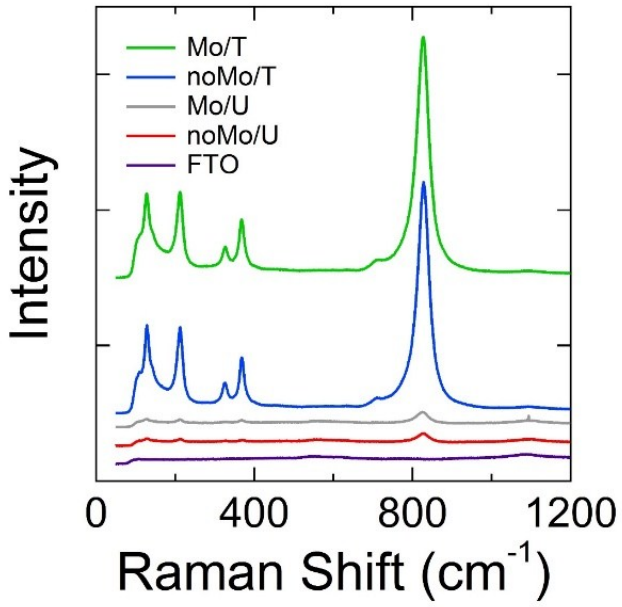

Figure S18. Raman spectra of the four types of BVO films on FTO substrates as well as a bare FTO substrate. Spectra are offset but unscaled. Acquisition conditions: 532 nm, 5% power, 10 s integration, normal incidence and collection.

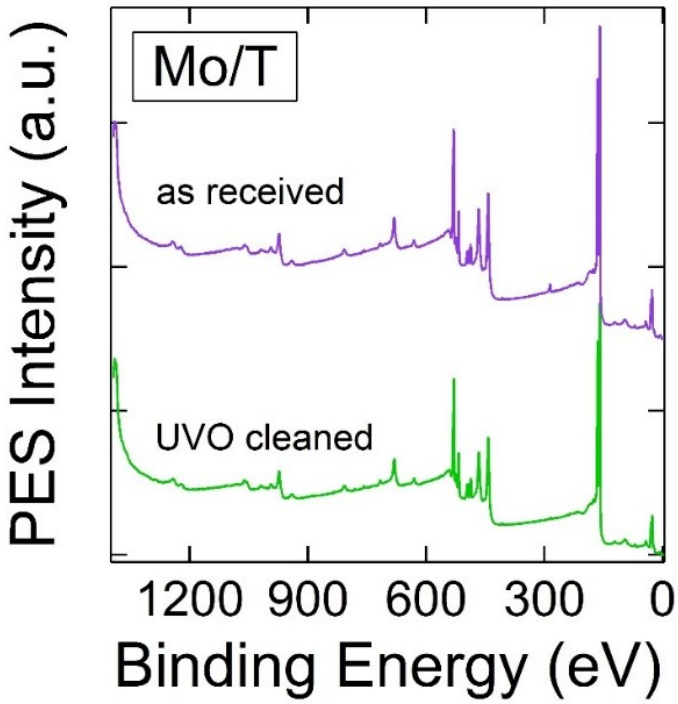

Figure S19. XPS survey spectra of a typical Mo/T film both before ("as received") and after rinsing in deionized water and *ex situ* cleaning by ultraviolet/ozone treatment ("UVO cleaned"). Only Bi, V, O, C, Mo, Na, and Sn (from FTO) were detected. UVO cleaning significantly reduced the carbon contamination.

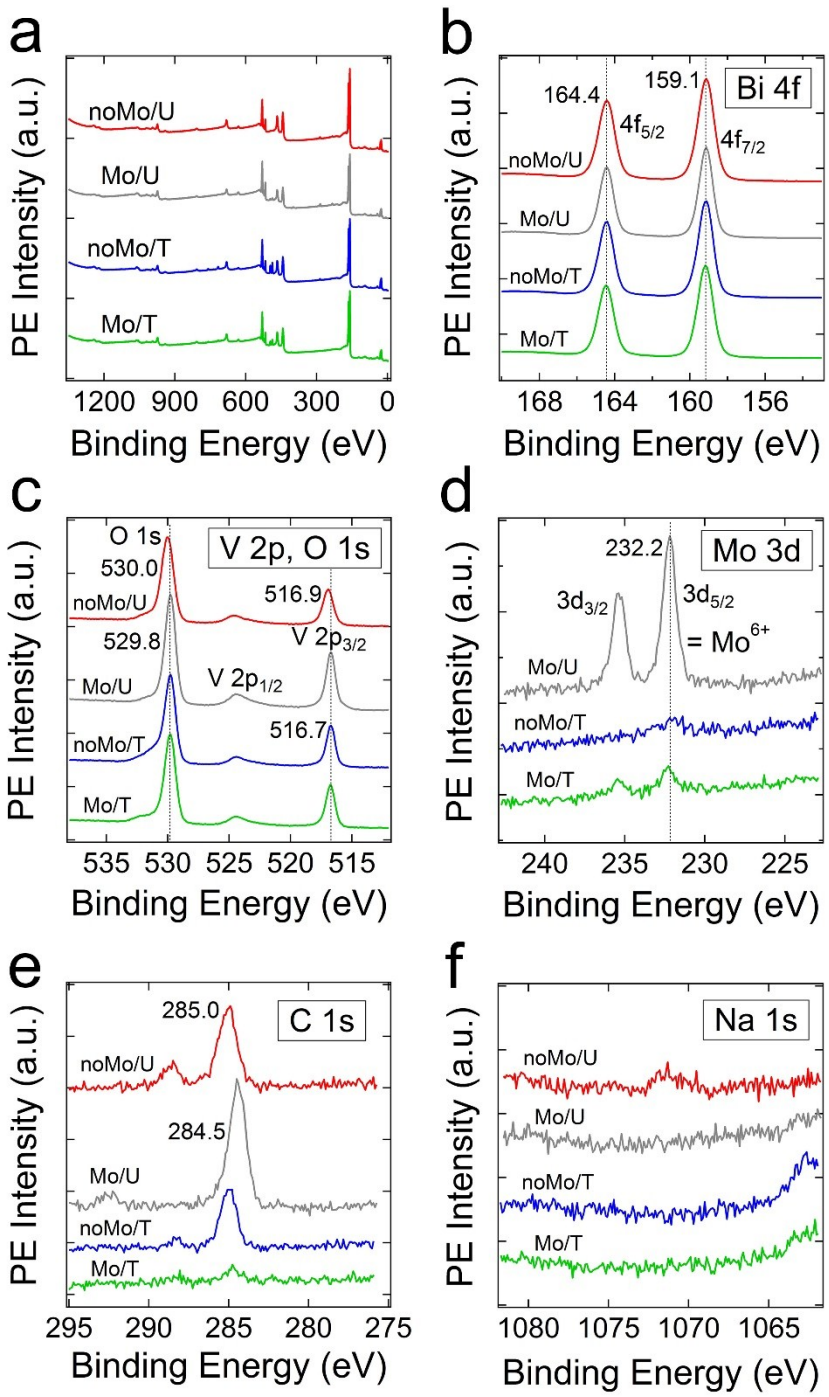

Figure S20. XPS data for UVO-cleaned BVO films. (a) Survey scans. Only Bi, V, O, C, Mo, Na, and Sn (from FTO) were detected. High-resolution elemental scans of (b) Bi, (c) V and O, (d) Mo, (e) C, and (f) Na. Spectra before and after cleaning were indistinguishable except for a larger C and (sometimes) Na signal from the as-received samples.

The following tables summarize the elemental composition of the Mo/T and noMo/U films as determined by XPS. Analyses were performed on both as-received and UVO-cleaned films.

Table 1a
Mo/T film. Data workup without carbon.

Treatment	XPS file	Atomic Concentration (%)			
		bismuth	vanadium	oxygen	molybdenum
As received	x140508_6	23.4	11.5	65.0	0.2
DI/UVO	x140507_1	23.1	11.9	64.8	0.2

Table 1b
Mo/T film. Data workup including carbon.

Treatment	XPS file	Atomic Concentration (%)				
		bismuth	vanadium	oxygen	moly	carbon
As received	x140508_6	20.9	10.3	58.2	0.2	10.5
DI/UVO	x140507_1	22.7	11.7	63.6	0.2	1.9

Table 2a
noMo/U film. Data workup without carbon or sodium.

Treatment	XPS file	Atomic Concentration (%)		
		bismuth	vanadium	oxygen
As received	x130729_1	26.7	11.3	61.9
DI/UVO	x130730_1	26.4	11.3	62.4

Table 2b
noMo/U film. Data workup including carbon and sodium.

Treatment	XPS file	Atomic Concentration (%)				
		bismuth	vanadium	oxygen	carbon	sodium
As received	x130729_1	21.5	9.1	49.8	15.9	3.6
DI/UVO	x130730_1	23.8	10.2	56.4	9.6	0.0

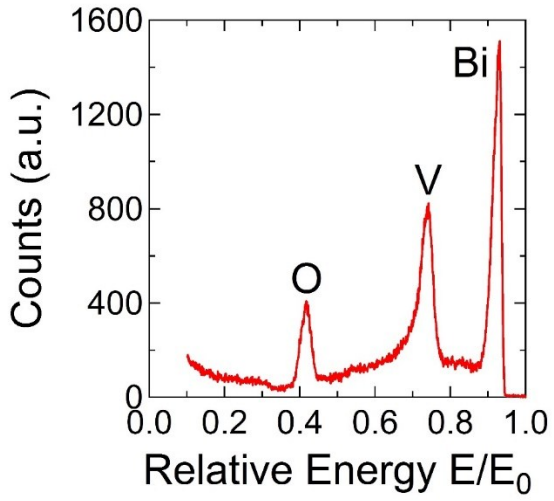

Figure S21. He^+ ion scattering spectrum of a Mo/T BVO film. The film was "as received" without UVO cleaning. Primary He^+ energy was 1 keV. Scattering angle = 135°. Pass energy = 160 eV. Note that hydrogen, while undoubtedly present on the surface, cannot be detected in this backscattering experiment.

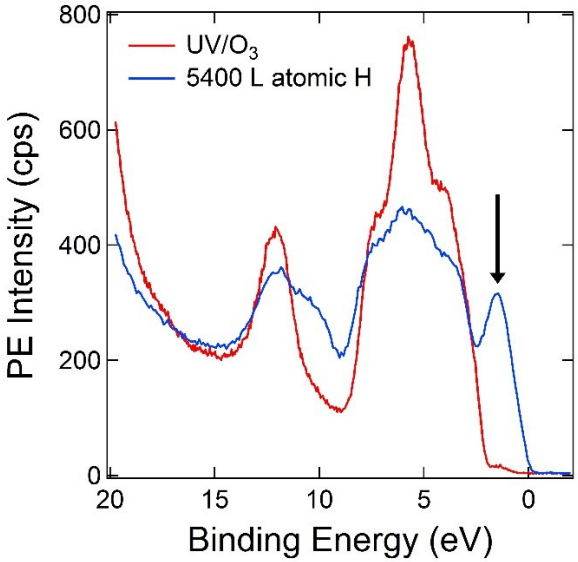

Figure S22. X-ray excited valance band spectra of a UV/ozone cleaned noMo/U film before (red) and after (blue) a 5400 Langmuir dose of atomic hydrogen. The H atoms reduce the BVO surface and cause a large increase in the in-gap peak (labeled with arrow).

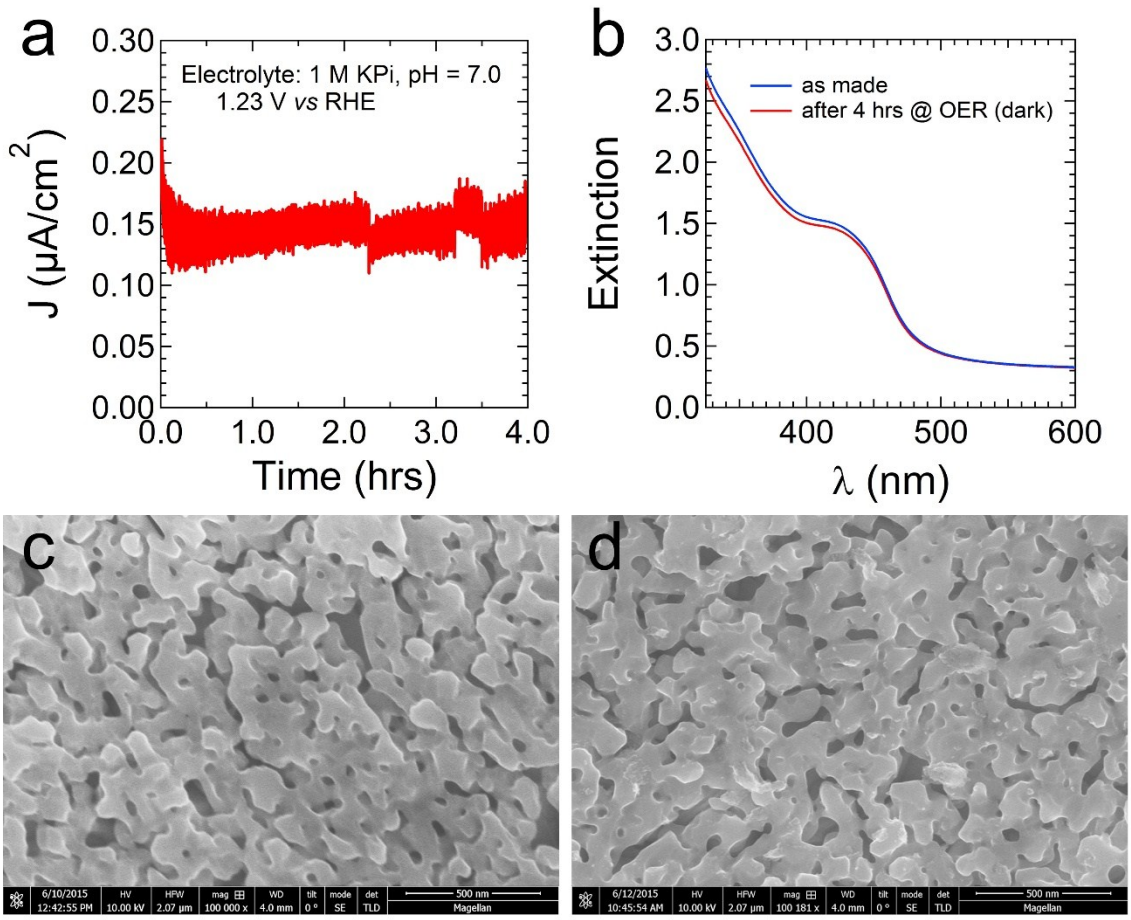

Figure S23. Stability of Mo/T films in water in the dark. (a) Current density versus time for an electrode held for 4 hours at 1.23 V_{RHE} in 1.0 *M* KH_2PO_4 at pH 7.0. (b) Optical extinction spectra of the electrode before and after the 4 hour treatment. SEM images of the film (c) before and (d) after the treatment, showing what appears to be slight etching.

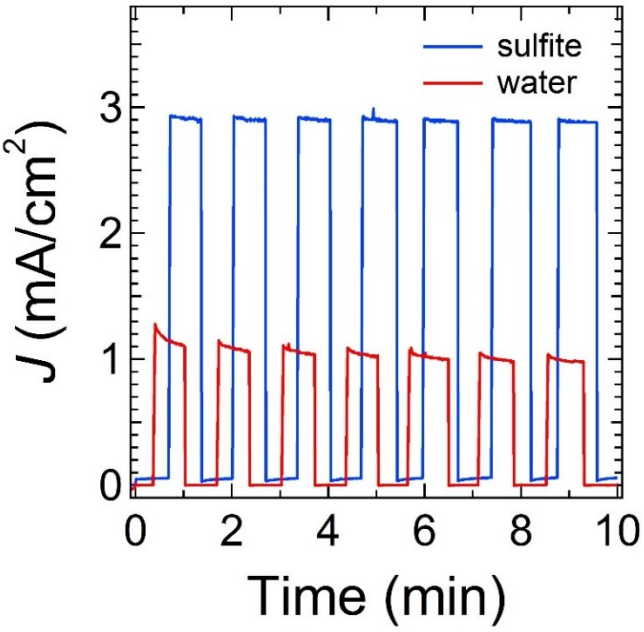

Figure S24. Current density vs. time for Mo/T electrodes in sulfite and water under chopped 1 sun illumination. Conditions: EE illumination, 1.23 V_{RHE}. The electrodes were biased under illumination for 3 minutes prior to acquiring the data.

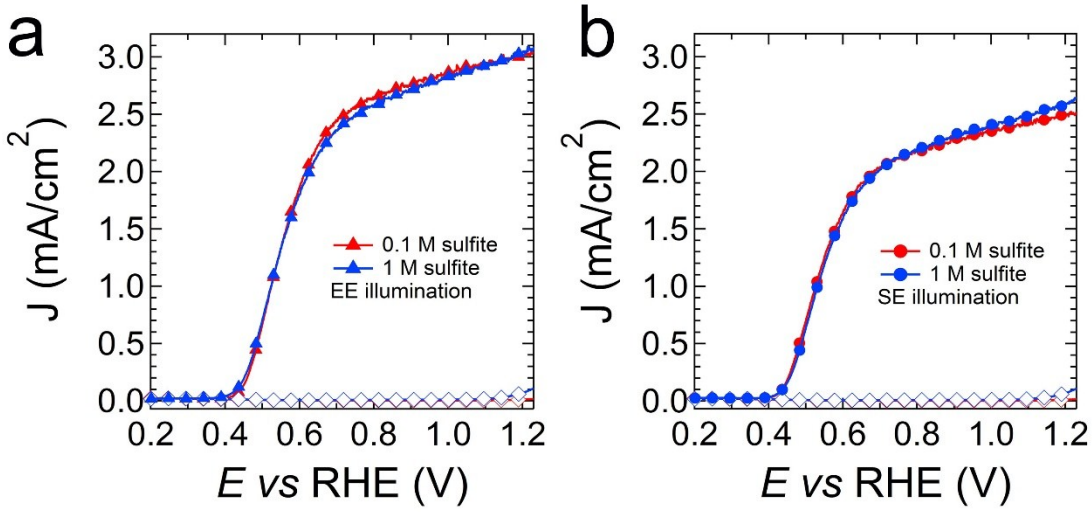

Figure S25. *J-V* curves for Mo/T films in 0.5 *M* K_2PO_4 buffer containing two different concentrations of Na_2SO_3.

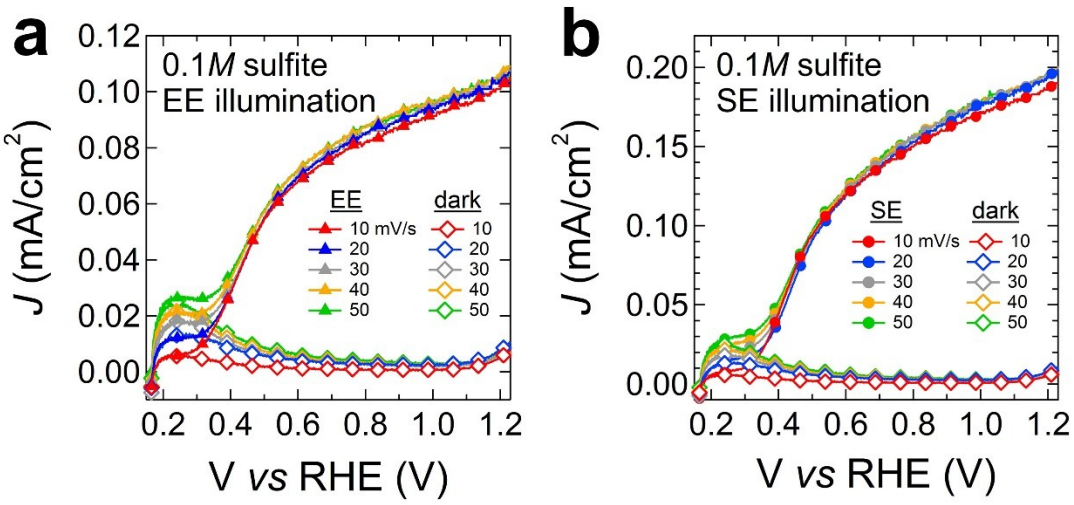

Figure S26. *J-V* curves as a function of bias scan rate for noMo/U films in sulfite under (a) EE illumination and (b) SE illumination.

References

[1] Z. Zhao, Z. Li and Z. Zou, Electronic structure and optical properties of monoclinic clinobisvanite $BiVO_4$. *Phys. Chem. Chem. Phys*., 2011, **13**, 4746-4753.

[2] J. Chen, *Spectroscopic ellipsometry studies of II-VI semiconductor materials and solar cells*, Ph.D. Thesis, The University of Toledo, 2010.